NAL TR-1140T

ISSN 0389-4010
UDC 533. 69. 04
533. 694. 2

TECHNICAL REPORT OF NATIONAL AEROSPACE LABORATORY

TR-1140T

Experimental Studies of Vortex Flaps and Vortex Plates Part. 1 0.53m Span 60° Delta Wing

Kenichi RINOIE

March 1992

NATIONAL AEROSPACE LABORATORY

CHŌFU, TOKYO, JAPAN

Experimental Studies of Vortex Flaps and Vortex Plates Part 1. 0.53 m Span 60° Delta Wing*

Kenichi RINOIE*1

ABSTRACT

Low-speed wind tunnel tests were conducted to investigate the flow around a leading-edge vortex flap at the maximum lift to drag (L/C) condition, and also to measure the performance of an inverted vortex flap and vortex plate. Associated force measurements and flow visualization tests were carried out on a 60 degree delta wing model. Results indicate that the maximum lift to drag ratio for any given flap deflection angle occurs when the flow smoothly comes onto the deflected vortex flap without forming a large leading-edge separation vortex on the flap surface. Use of a vortex plate was found to reduce the drag in comparison to the datum wing, a benefit due to some leading-edge suction acting on the forward facing region between the delta wing and the vortex plate.

Keywords: low-speed aerodynamics, delta wing, vortex flap, votex plate, leading-edge separation vortex

概　　要

前縁ボルテックス・フラップまわりの流れを調べるために低速風洞実験を行った。逆ボルテックス・フラップとボルテックス・プレートの特性も計測した。後退角60°のデルタ翼模型を用いて空気力測定と流れの可視化を行った。

その結果，折り曲げたボルテックス・フラップ表面上に大きな前縁剥離渦を形成しない特定の迎角において，デルタ翼の揚抗比が最大になることが示された。またボルテックス・プレートを用いると抗力が減少することが示された。これは翼前方へ働く吸引力が，デルタ翼とボルテックス・プレートとの間の領域に存在するためである。

Nomenclature

AR Aspect ratio
Cr Wing centre-line chord
C_D Drag coefficient
C_{D0} C_D at zero lift
C_L Lift coefficient
g Vortex plate leading-edge position measured from leading-edge of the wing in the chordwise direction
H.L. Hinge line
K Induced drag coefficient
L/D Lift/Drag ratio
R Reattachment line
Re_{cr} Reynolds number (based on wing centre-line chord)
S Secondary separation line
U_∞ Free stream velocity

*Received 24 December, 1991
*1 Advanced Aircraft Research Group

α Wing incidence

δ_f Vortex flap deflection angle measured normal to the hinge line

1. Introduction

A sharp-edged delta wing is often used for supersonic cruise aircraft because of its good supersonic performance. At subsonic speeds and particularly at take-off and landing, it is necessary for the delta wing aircraft to fly at a high incidence, in order to generate sufficient lift. At high incidence the flow separates from the leading-edges of the wing, wraps up and forms a pair of vortices over the upper surface. Each vortex is called a leading-edge separation vortex. The leading-edge separation vortex produces a large suction force over the wing which increases the lift component. However, there is also a high drag component associated with this suction force. Therefore the lift/drag ratio of the delta wing at low speeds is relatively poor.

The leading-edge vortex flap (LEVF) is one of the devices which can improve the aerodynamic efficiency of delta wings at low speeds (ref. 1). The LEVF is a full span deflectable flap attached to the leading-edge of the delta wing. With the flap deflected downward, a leading-edge separation vortex can be formed over the forward facing flap surface, as is shown in Fig. 1a. The vortex suction force acting normal to the flap surface generates a thrust component. Hence it reduces the drag of the wing and improves the lift/drag ratio at a given lift coefficient, which is essential to the improvement of the take off and climb performance of delta wing aircraft.

Many tests have been done which confirm the benefit of the LEVF (refs. 1, 2 and 3). Ref. 4 presents an overview of recent LEVF research. Tests have been made at the College of Aeronautics, Cranfield Institute of Technology (refs. 5, 6 and 7) using two 60° delta wing models with tapered vortex flaps, in order to study the optimum flap size and the optimum flap deflection angle. All these experiments (refs. 1-7) showed that the LEVF can give appreciable

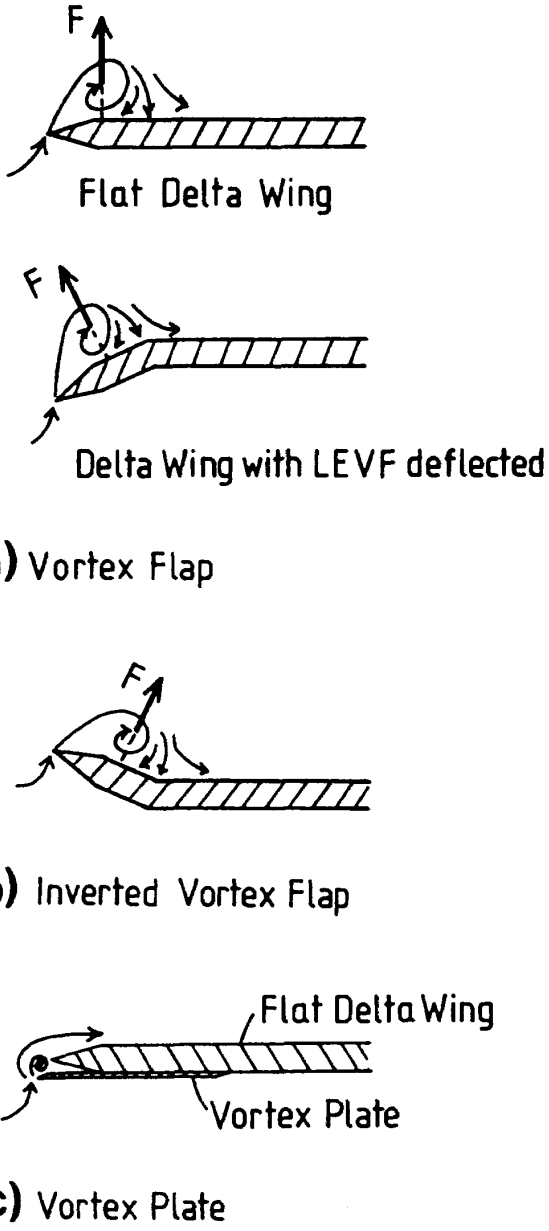

Fig. 1 Concept of Vortex Flap and Vortex Plate

improvements in the lift/drag ratio over a wide range of incidence and confirmed the potential benefit of the vortex flap. It was suggested in ref.1 that the best *L/D* performance is obtained when the flow separates at the leading edge of the vortex flap and reattaches near the wing-flap hinge line. Thus the spiral leading-edge vortex is located entirely over the flap as is shown in Fig. 1a. However, it was suggested in ref. 7 that the optimum lift to drag ratio is achieved with the flow coming smoothly onto the deflected LEVF, i.e. there is no vortex above or below the flap surface.

In this paper, experiments were conducted to gain more understanding of the complex flow around

the LEVF. The delta wing model tested is the same as used in ref. 5. Three different flap deflection angles were used in order to study the flow pattern differences around the LEVF.

When the LEVF is deflected upward instead of downward, it is expected that the leading-edge separation vortex would be formed at a lower incidence than for the normal wing (Fig. 1b). This vortex can increase not only the drag but also the lift at a low incidence. This large lift and drag component at low incidence might be helpful for the landing situation (ref. 8). Hence in this report the inverted LEVF configuration was also tested.

Rao & Johnson (ref. 9) showed that a vortex plate, a type of leading-edge split flap, can also give substantial amounts of leading-edge thrust. The vortex plate is a thin plate attached to the lower surface of the leading-edge of the delta wing as is shown in Fig. 1c. At positive incidence separation occurs at the leading-edge of the vortex plate and at a particular incidence a spanwise vortex can form just in front of the leading-edge of the wing with the reattachment line along the leading-edge. This vortex induces a suction in the cavity between the delta wing and the vortex plate and so reduces the drag. In this paper, tests were made to improve the understanding of how the vortex plate works.

In summary, the purpose of this research is

1) to gain more understanding of the flow around the LEVF, in order to determine the condition for the optimum *L/D*,

2) to discover the characteristics of the inverted vortex flap,

3) to investigate the benefits of the vortex plate.

This research was done at the College of Aeronautics, Cranfield Institute of Technology, U.K., while the author was staying in the College for a period of one year starting October 1990 with the aid of the S.T.A. research abroad fellowship.

2. Experimental Details

Fig. 2 shows the model details. This model is the same one that was tested in ref. 5. The model is

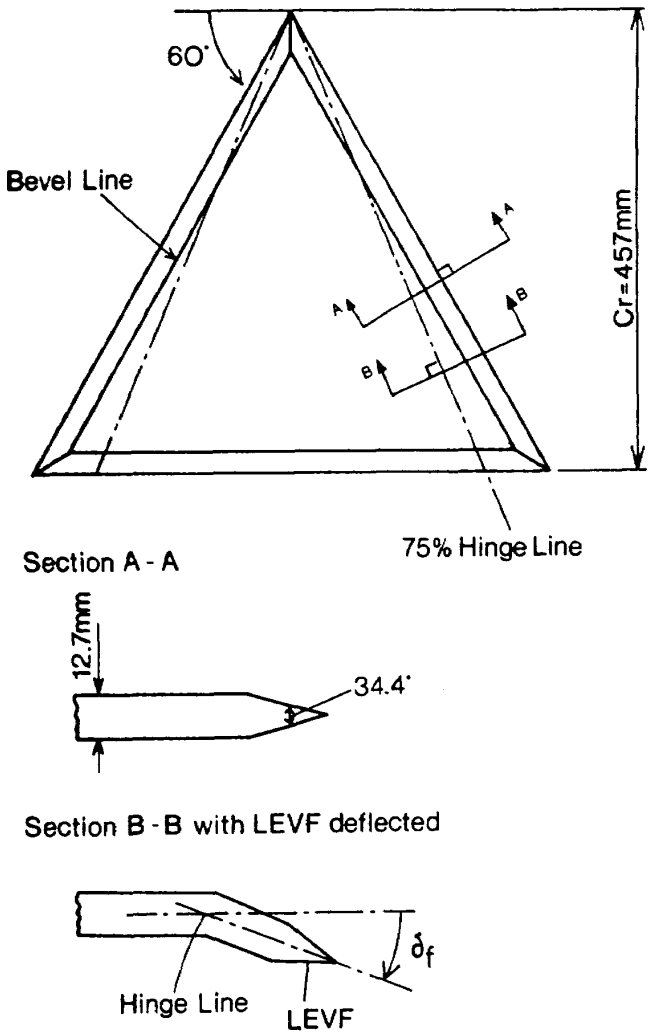

Fig. 2 Delta Wing Model with LEVF

a 60° flat delta wing having no camber. The centre line chord length *Cr* is 457 mm and the thickness is 12.7 mm. The model is made of plywood. The upper and lower surfaces of all edges are cut away so that the edges are sharp and have an apex angle of 34.4°, where this angle is measured in a plane normal to the edge concerned. The model has the LEVF hinge lines running from the wing apex to 75% of the trailing-edge semispan station. In ref. 5, two different model types which have 50% and 75% hinge line were tested. Results showed the 75% model has a better performance than that of the 50% model. Therefore, only the 75% hinge line model was used in this experiment. In ref. 5, several configurations which have different flap deflection angle δ_f were tested. The angle δ_f is defined as the angle between the mean line of the inboard wing and that of the LFVF, measured in the plane

normal to the hinge line. The sign of δ_f is positive when the LEVF is deflected downward. It was shown in ref. 5 that the maximum *L/D* was achieved with δ_f = 10°. In order to study the flow differences between the optimum configuration and those with larger flap deflection angles, the flap configurations δ_f = 10°, 15° and 30° were tested. The inverted LEVF cases were measured at δ_f = −10° and −30°.

The vortex plate (Fig. 3) is made of 1 mm thickness aluminum plate and has a sharp leading-edge. The plan shape is the same as that of the leading-edge region of the delta wing model and the width of the plate is 48 mm. The plate was attached to the lower surface of the datum model (no LEVF deflection). The plate can be moved forward as shown in Fig. 3. The position of the plate is defined by the chordwise distance *g* between the leading-edge of the wing and that of the vortex plate. In these tests the plate was set at *g/Cr* = 0., 0.01 and 0.02. The position *g/Cr* = 0. means that the leading-edge of the vortex plate coincides with the leading-edge of the wing in plan view.

The experiments were done in the 1 m x 0.69 m low-speed open-jet wind tunnel. Lift and drag were measured using a T.E.M. three-component wind tunnel balance and the tunnel micro-computer data acquisition system. Measurements were made at tunnel speeds of U_∞ = 20 m/s and 30 m/s. The Reynolds numbers based on the wing centreline chord were 6.1 x 10^5 and 9.1 x 10^5, respectively. The incidence of the model α was increased from −14° until the stall occurred (about 34°). The model was mounted on twin shielded struts with a tail-sting for incidence control. A picture of the model, the tunnel balance and the wind tunnel is shown in Fig. 4.

The T.E.M. balance was calibrated before the experiments. The strut tare effect was taken into account and tunnel boundary corrections were applied to the measured data. The solid and wake blockage effects were corrected using the approximate method described in ref. 10. The lift effect was corrected according to ref. 11. The effect of static pressure gradient was neglected because

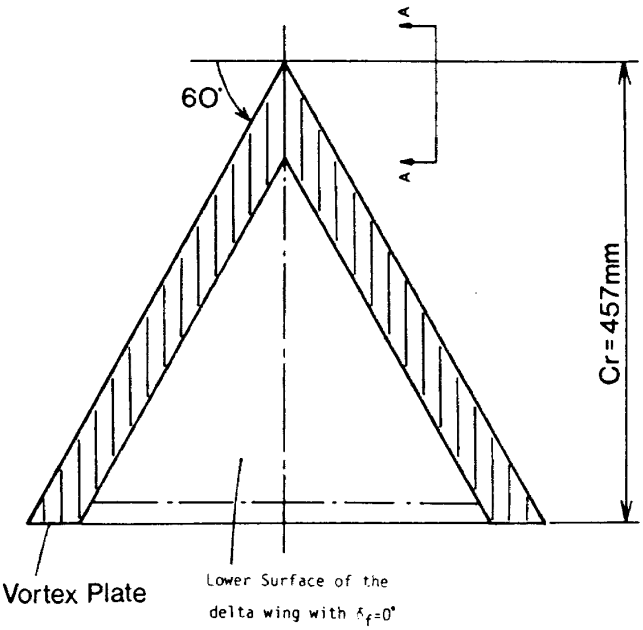

Fig. 3 Delta Wing Model with Vortex Plate

the tunnel is of the open-jet type. Interference between the struts and the model was not accounted for.

The aerodynamic coefficients were calculated for every flap deflection angle, based on the same total projected wing area with no LEVF deflection. In many studies, the vortex flap is attached to the leading-edge of the delta wing, which causes an increase in model area. In our tests a hinged flap was fitted and the datum delta wing area was used in calculating all aerodynamic coefficients. For the vortex plate measurements, the datum wing area was used as a basis, even though the total area of the model is greater than that of the datum wing for *g/Cr* = 0.01 and 0.02.

Flow visualization test using the surface oil flow, smoke filament and flying tuft techniques were very helpful in describing the flow around the LEVF.

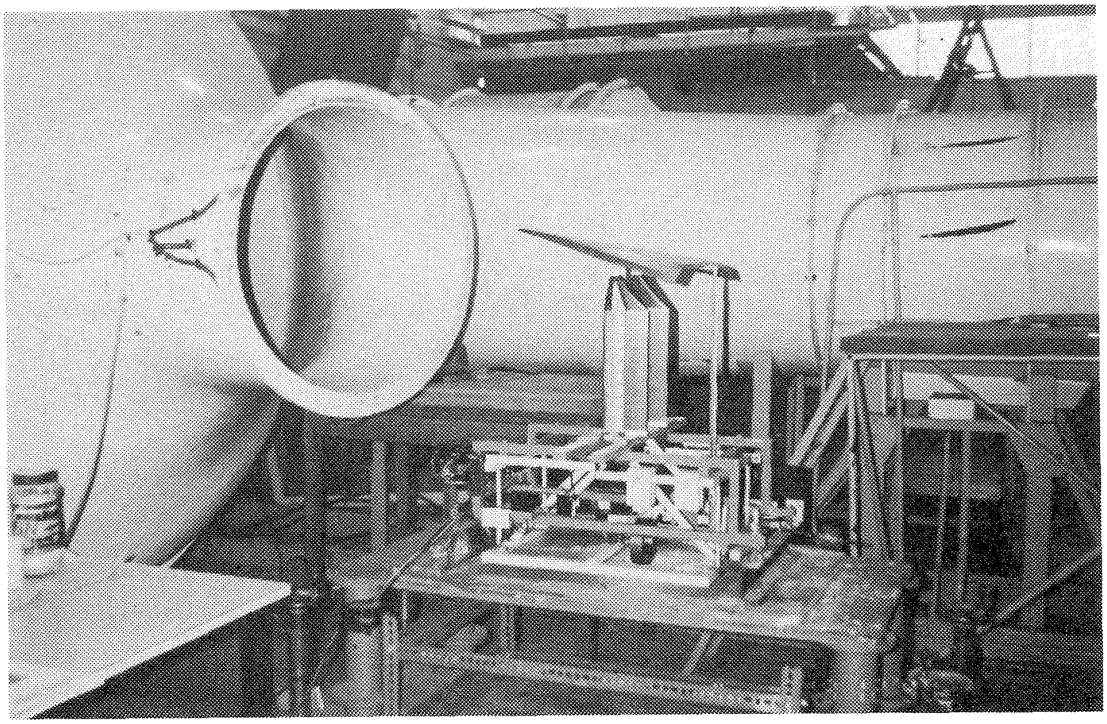

Fig. 4 Wind Tunnel, Model Mounting and Tunnel Balance

3. Results and discussion

3.1 Vortex Flap

The C_L vs. α curves are shown in Fig. 5 for various LEVF deflection angles δ_f at Reynolds numbers of 6.1×10^5 and 9.1×10^5. Because of load restrictions on the tunnel balance, incidences greater than about 15 deg at $Re_{cr} = 9.1 \times 10^5$ could not be used. Figure 5 shows that the C_L decreases as the LEVF is deflected downwards at both Reynolds numbers. Similarly the C_L increases as the LEVF is deflected upwards. Some 'bumps' are observed near the region of $\alpha = 0°$ ($\delta_f = 0°$), $\alpha = 5°$ ($\delta_f = 10°$) and $\alpha = 10°$ ($\delta_f = -30°$) for $Re_{cr} = 6.1 \times 10^5$. These 'bumps' diminish or reduce at the same incidence position for $Re_{cr} = 9.1 \times 10^5$. The separated shear layer on the wing at the lower Reynolds number is thicker than that at the higher Reynolds number and so may have a greater effect on the C_L vs. α curves at the lower value of Re_{cr}.

The C_L is not zero at $\alpha = 0°$ for the datum wing although the model is symmetrical. The reason for this is probably the two tunnel struts under the model which affect the flow pattern. Similarly the C_L-α curves for α positive and $\delta_f = -10°$ and $-30°$ should be similar to the curves for α negative and $\delta_f = 10°$ and $30°$. Any differences reflect the effects of strut interference.

Fig. 6 shows the C_D vs. α curves. Both Reynolds number cases show similar results. As δ_f increases the C_D decreases for most of the positive incidence region. Similarly C_D increases as the flap is deflected upward. Fig. 6 shows that the incidence when the C_D is a minimum, increases as the flap is deflected downwards. The reason is explained as follows. As is seen in Fig. 5, the incidence at which the C_L becomes zero increases, as the flap deflection angle increases. Usually the minimum drag is attained when the C_L is close to zero. Therefore, the incidence for the minimum C_D increases as δ_f increases.

Fig. 7 shows the lift to drag ratio (L/D) versus C_L. Both Reynolds number cases show similar results. Again any lack of symmetry (when expected) is probably due to strut interference. For flap deflection angles of 10° and 15°, the maximum L/D value is greater than that of the datum wing. The L/D attains an absolute maximum at $C_L = 0.25$ with $\delta_f = 10°$. This result agrees with that in ref. 5. The L/D ratios with $\delta_f = 10°$ and 15° are larger than those of the

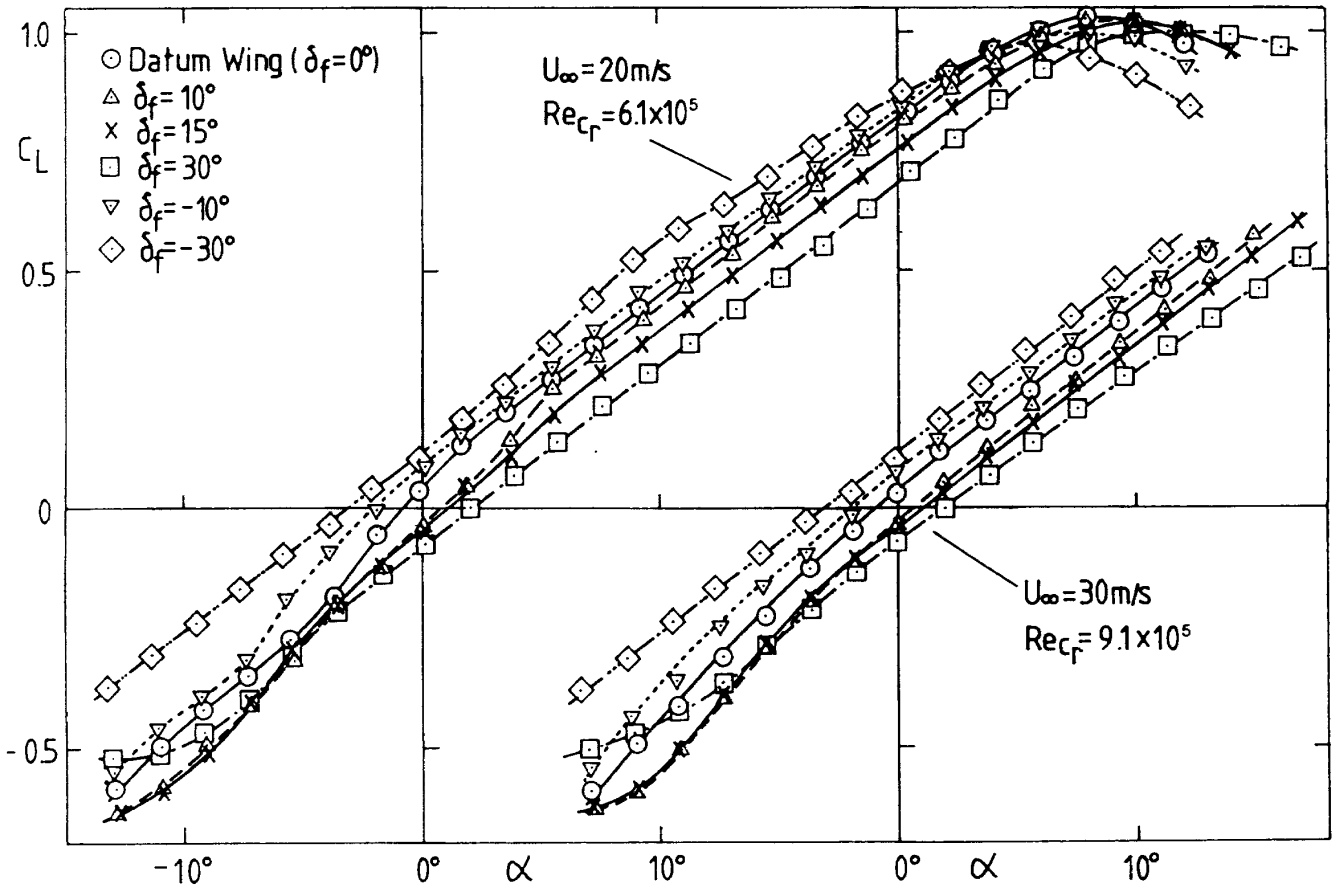

Fig. 5 Effect of LEVF on C_L vs. α

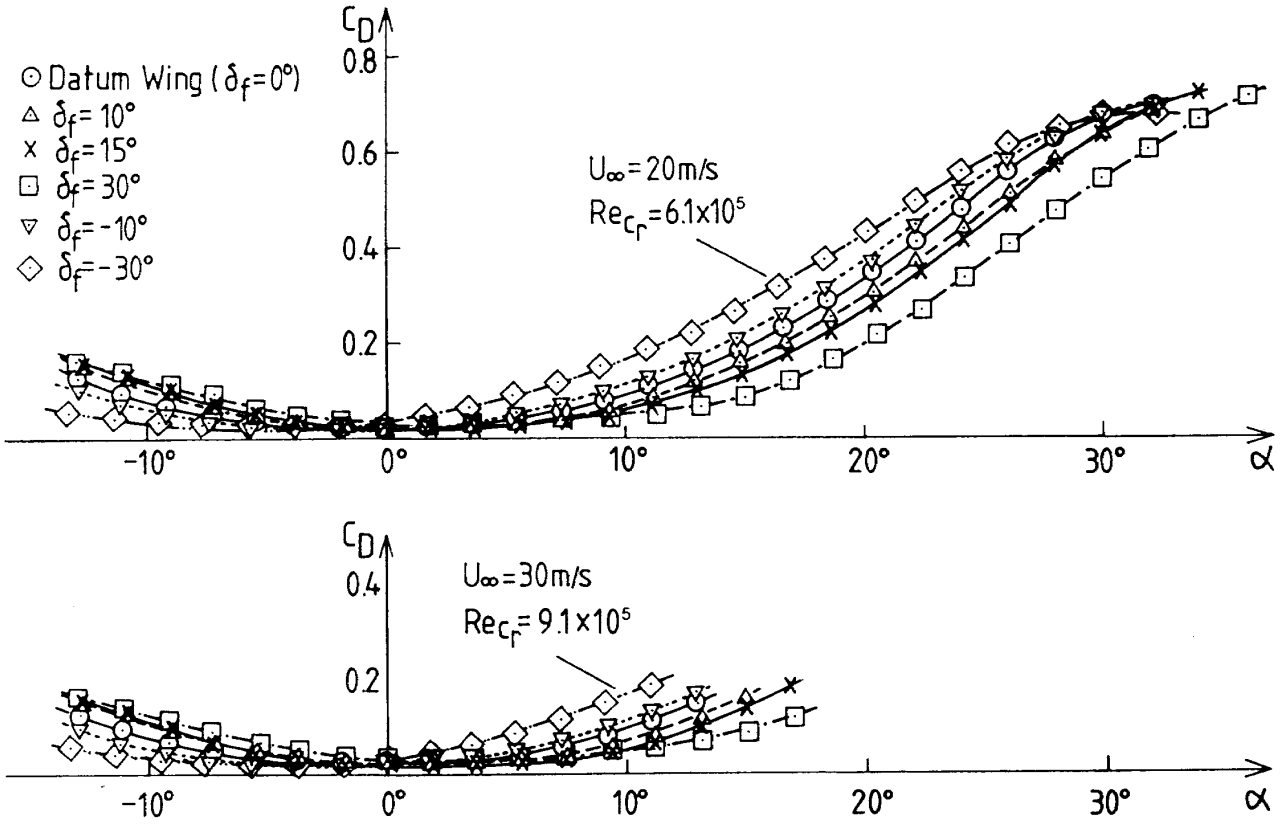

Fig. 6 Effect of LEVF on C_D vs. α

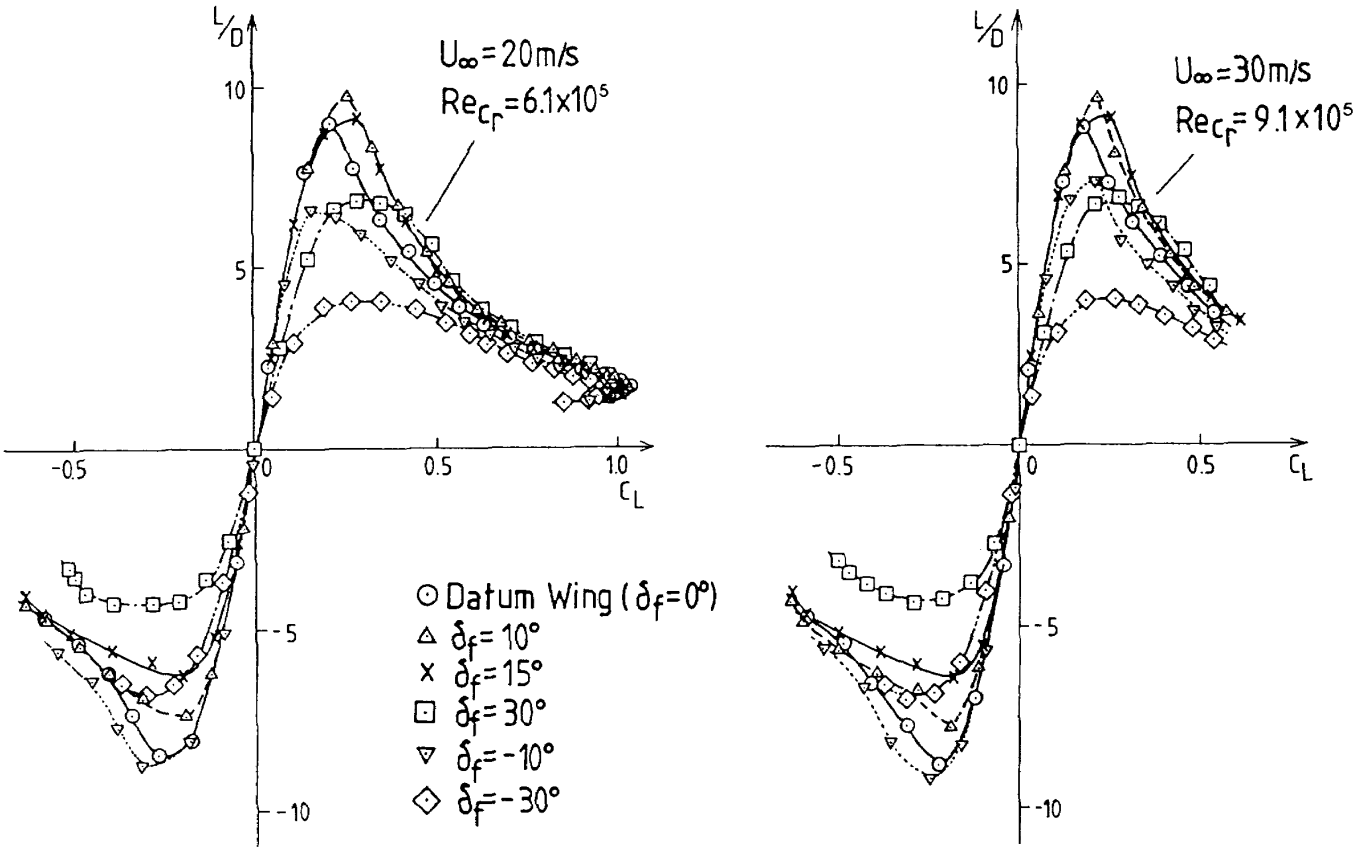

Fig. 7 Effect of LEVF on *L/D* vs. C_L

datum wing for all C_L's > 0.2.

Figs. 8 and 9 show the surface flow patterns sketched from oil flow pictures for both upper and lower surfaces at $Re_{cr} = 9.1 \times 10^5$. The patterns define the vortex positions on the wing and flap surfaces. In these figures, H.L. denotes the hinge line, R the reattachment line and S the secondary separation line of the vortex. The hatched region denotes a small separation bubble. In this bubble the oil moved very little. The flow separation region was confirmed by the smoke filament and flying tuft tests. In Fig. 8 ($\delta_f = 10°$), at an incidence of –3.6°, a leading-edge separation vortex, which is clearly recognized by the reverse flow region between reattachment line and secondary separation line, is formed on the lower surface. There is no vortex on the upper surface. The same flow should be formed at $\alpha = +3.6°$ with the vortex flap deflected upwards 10 degrees. From $\alpha = 0.1°$ to 5.6° there are only small separation bubbles (hatched region) and the flow comes smoothly onto the flap with no large vortex being formed on either surfaces. At $\alpha = 7.5°$ the leading-edge separation vortex is observed in the tip region of the upper surface. At $\alpha = 9.3°$ a large separation vortex is formed over the whole of the vortex flap upper surface.

In Fig. 9 ($\delta_f = 30°$), at the incidences –3.6° and 2.0°, the leading-edge separation vortex is formed on lower surface of the model. At $\alpha = 5.7°$, on the upper surface, it flows smoothly over the flap surface but a separation occurs near the flap hinge line and the separation vortex is formed over the wing. The same tendency is seen at $\alpha = 9.5°$. At $\alpha = 13.2°$ and 15.1°, where the visualization was done only on the upper surface, the reverse flow region is observed not only on the wing surface but also on part of the vortex flap. Thus at high incidences a large leading-edge vortex covers much of the model top surface.

Figs. 10 and 11 show some C_D vs. C_L curves together with the corresponding flow pattern sketches in the transverse plane. These were deduced from flow visualization using the smoke filament and surface oil flow patterns (Figs. 8 and 9). In Fig. 10, at $\delta_f = 10°$ from $\alpha = 0.1°$ to 5.6° there is only a

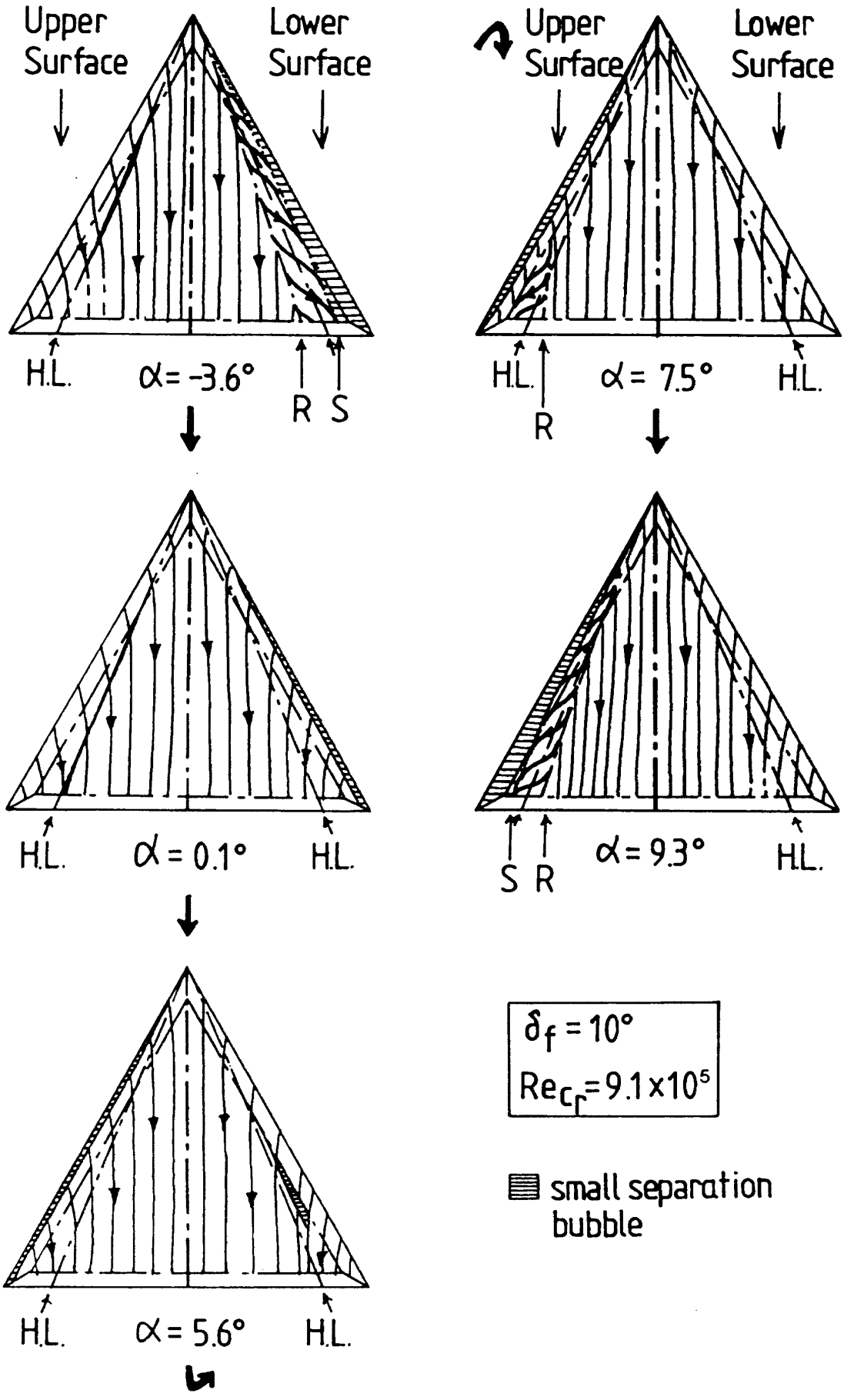

Fig. 8 Surface Flow Patterns (δ_f=10°)

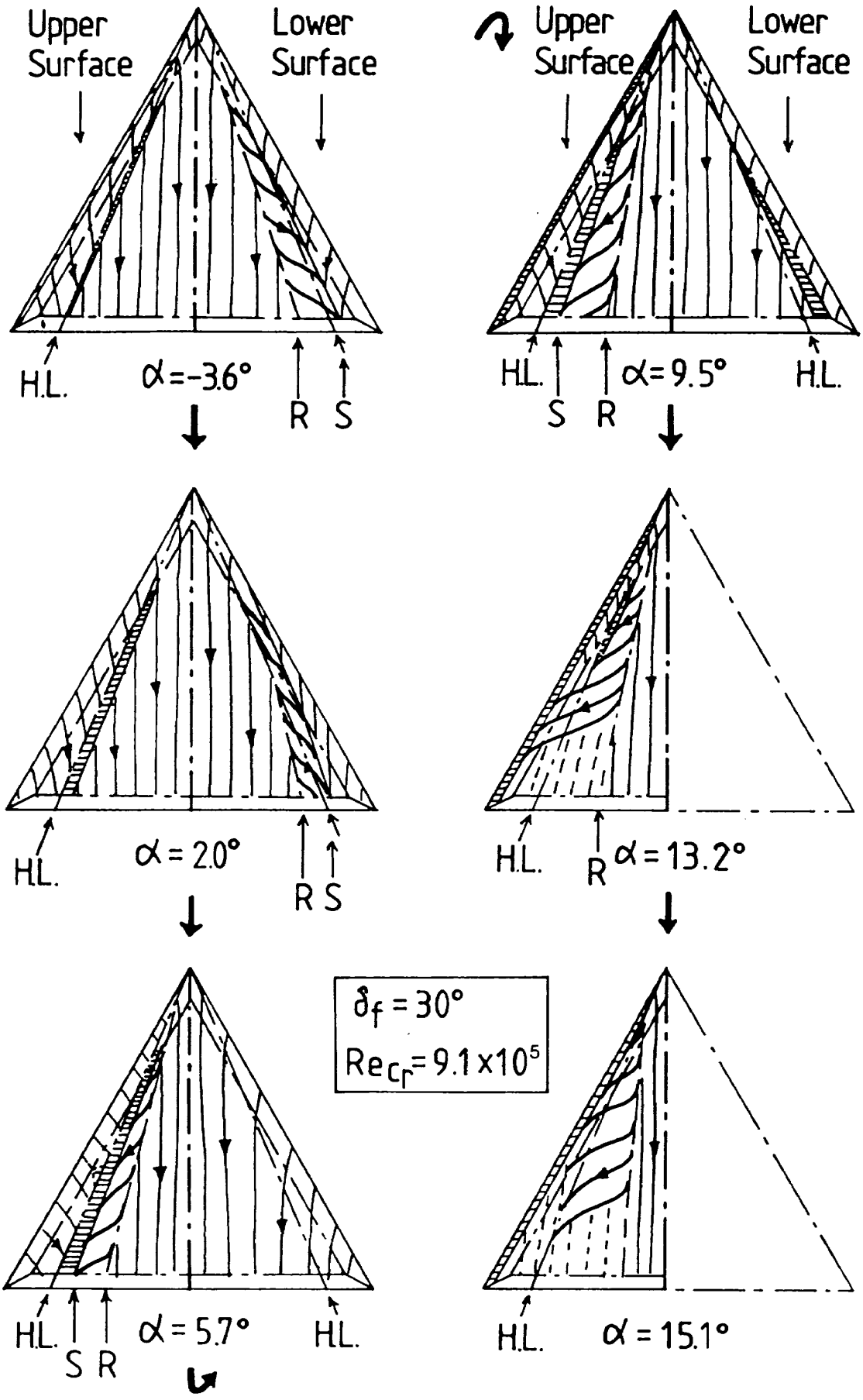

Fig. 9 Surface Flow Patterns (δ_f=30°)

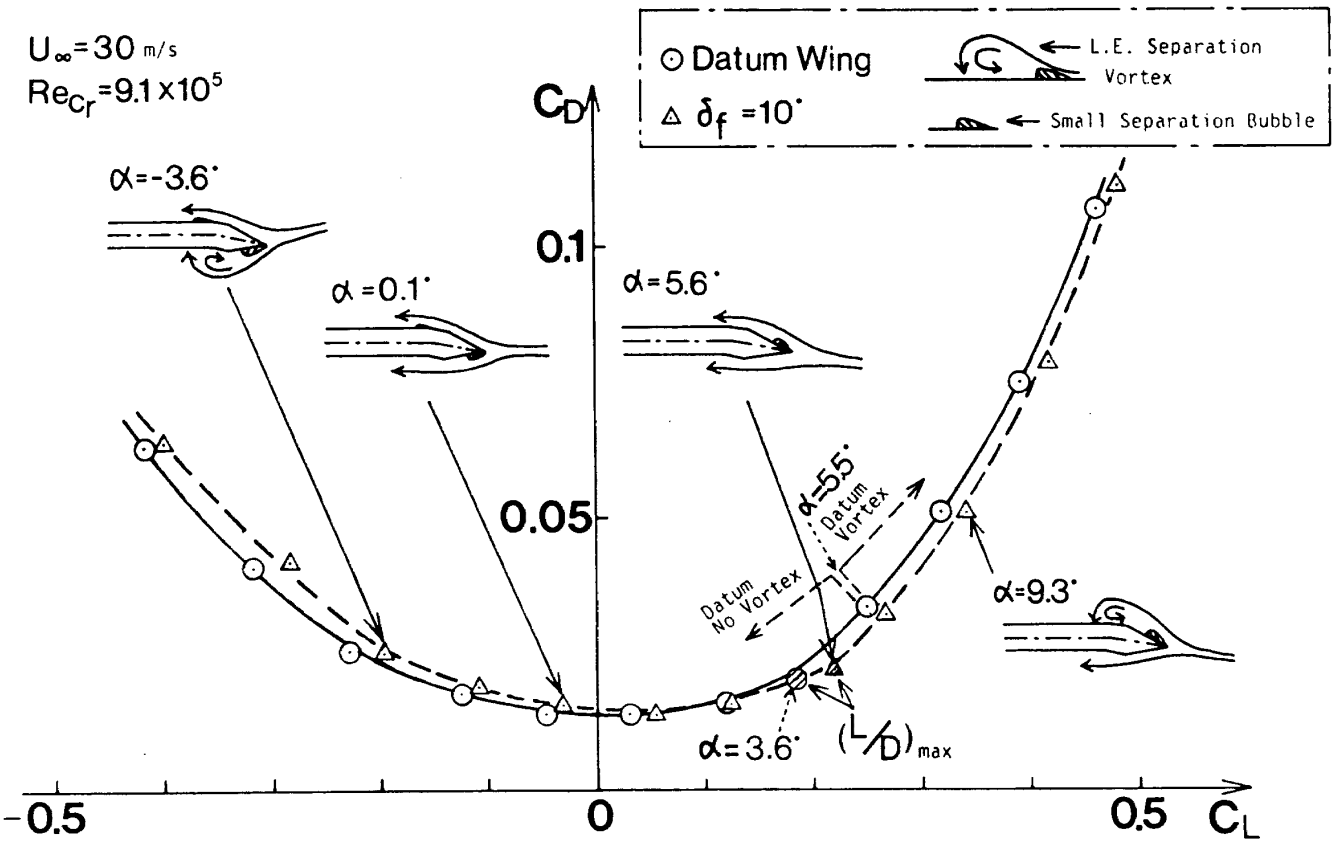

Fig. 10 C_D vs. C_L and Cross Flow Patterns (δ_f=10°)

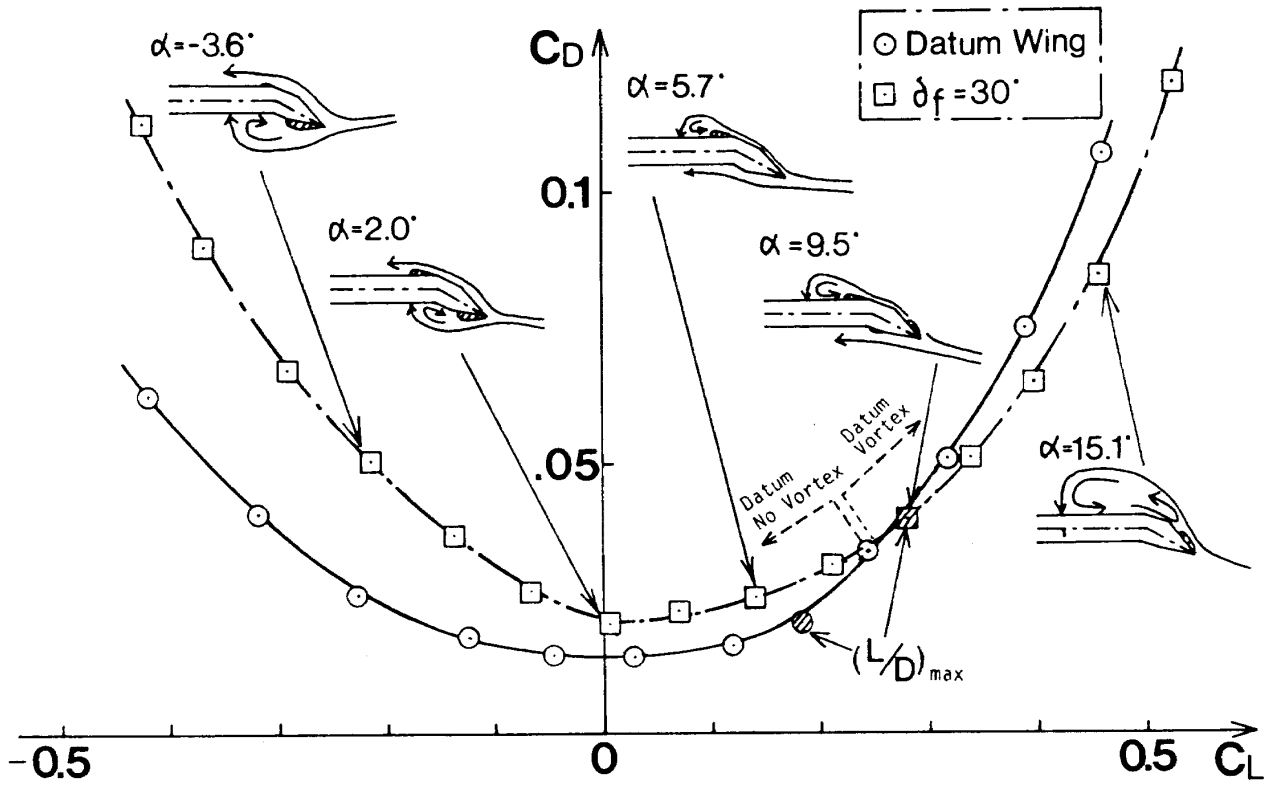

Fig. 11 C_D vs. C_L and Cross Flow Patterns (δ_f=30°)

small separation bubble on the upper surface and the flow comes smoothly onto the flap with no large vortex being formed. For the datum wing, it was observed in flow visualization tests that the leading-edge separation vortex begins to form at $\alpha = 5.5°$. For $\delta_f = 10°$, the *L/D* attains the maximum value when the incidence is 5.6° with no large vortex being formed. The non-existence of the large separation vortex at this incidence means that the wing has a smaller drag than that for the datum wing on which the leading-edge separation vortex is formed at almost the same incidence. Fig. 10 shows that C_D at $\alpha = 5.6°$ for $\delta_f = 10°$ is almost the same as that for the datum wing at $\alpha = 3.6°$ when there is no leading-edge separation vortex, and the datum wing achieves its maximum *L/D* ratio. However, C_L at $\alpha = 5.6°$ for $\delta_f = 10°$ is larger than that of the datum wing at $\alpha = 3.6°$, because of the higher incidence. Hence this larger C_L at a similar value of C_D makes *L/D* for $\delta_f = 10°$ much higher than that of the datum wing.

At higher incidence eg $\alpha = 9.3°$, it is seen that the leading-edge separation vortex is formed over the wing and flap surface. The suction effect of the vortex, formed on the forward facing flap surface, causes the C_D to be smaller than that of the datum wing, as was explained in ref. 1.

With the larger vortex flap deflection of 30° (Fig. 11), when C_L is less than 0, the leading-edge separation vortex is formed under the wing causing a large increase in C_D over that of the datum wing. From $\alpha = 5.7°$ to 9.5° it is observed that the flow comes smoothly onto the deflected leading-edge without forming a large leading-edge separation vortex on the flap surface. However, the flow does separate at the flap hinge line and the vortex is formed inboard of that line. For the datum wing, the same C_L as at $\alpha = 5.7°$ to 9.5° for $\delta_f = 30°$ is attained at lower incidence (α is less than 5.5°), and at these incidences it was observed that there is no leading-edge separation vortex on the datum wing. The existence of the vortex on the inboard wing for $\delta_f = 30°$ causes much higher drag than that of the datum wing. The maximum *L/D* for $\delta_f = 30°$ is achieved at an incidence of 9.5, but because of the inboard vortex, the value of $(L/D)_{max}$ is lower than that for $\delta_f = 10°$. At $\alpha = 15.1°$ where a large leading-edge separation vortex is formed on the flap as well as on the wing, the suction effect over the flap surface reduces C_D below that of the datum wing. Consequently *L/D* is larger as shown in Fig. 7.

3.2 Vortex Plate

Fig. 12 shows the C_L vs. α curves for various chordwise vortex plate positions together with the datum wing. It is seen that the results at $Re_{cr} = 6.1 \times 10^5$ and 9.1×10^5 are almost the same. The effect of the vortex plate at any of the three positions tested is quite small at positive incidence.

When the incidence is between −5° and −14°, the C_L is reduced below that of the datum wing. A strong vortex is observed by the flow visualization tests on the lower surface of the vortex plate and the wing. This increased suction substantially reduces the lift (i.e. increases the lift downwards). This suggests that the better lift component would be gained, when the vortex plate is attached to the upper surface of the datum model.

Fig. 13 shows the C_D vs. α curves. Again, there is little difference between the results at $Re_{cr} = 6.1 \times 10^5$ and 9.1×10^5. However this figure does show that the drag with the vortex plate fitted is smaller than that of the datum wing at positive incidences, which agrees with the results in ref. 9. For negative incidences the C_D values with vortex plates fitted are greater than that of the datum wing because of the existence of the strong leading-edge separation vortex on the lower surface of the vortex plate.

Fig. 14 illustrates the lift to drag ratio versus C_L for the vortex plate fitted to the wing. Results show that the maximum value of *L/D* is reduced in comparison with the datum wing for both Reynolds number cases. However, it is seen that the *L/D* ratio is improved for all C_L values greater than about 0.35, especially for the case of $g/Cr = 0.02$. It is noted that the effect of wing area increase

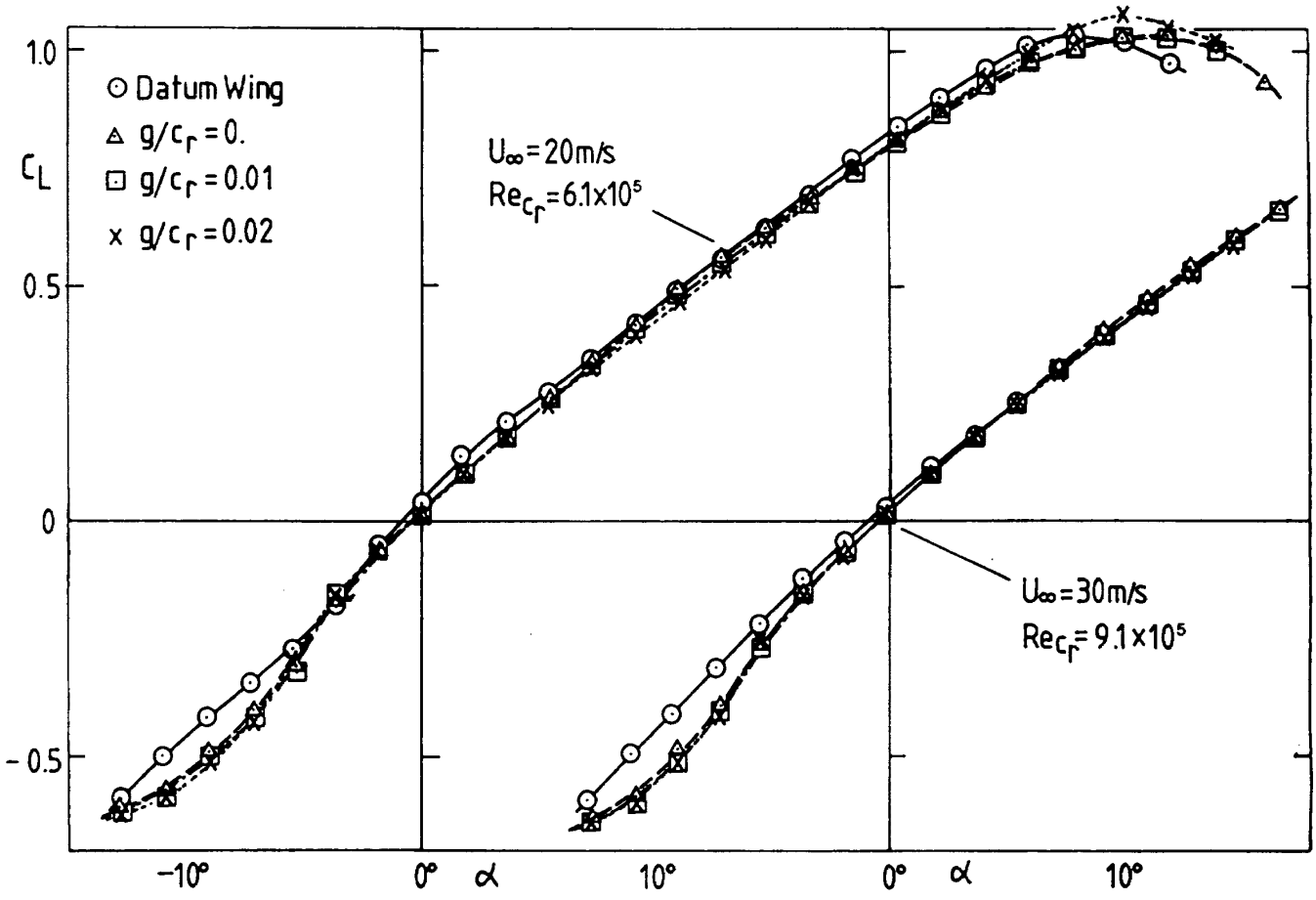

Fig. 12 Effect of Vortex Plate on C_L vs. α

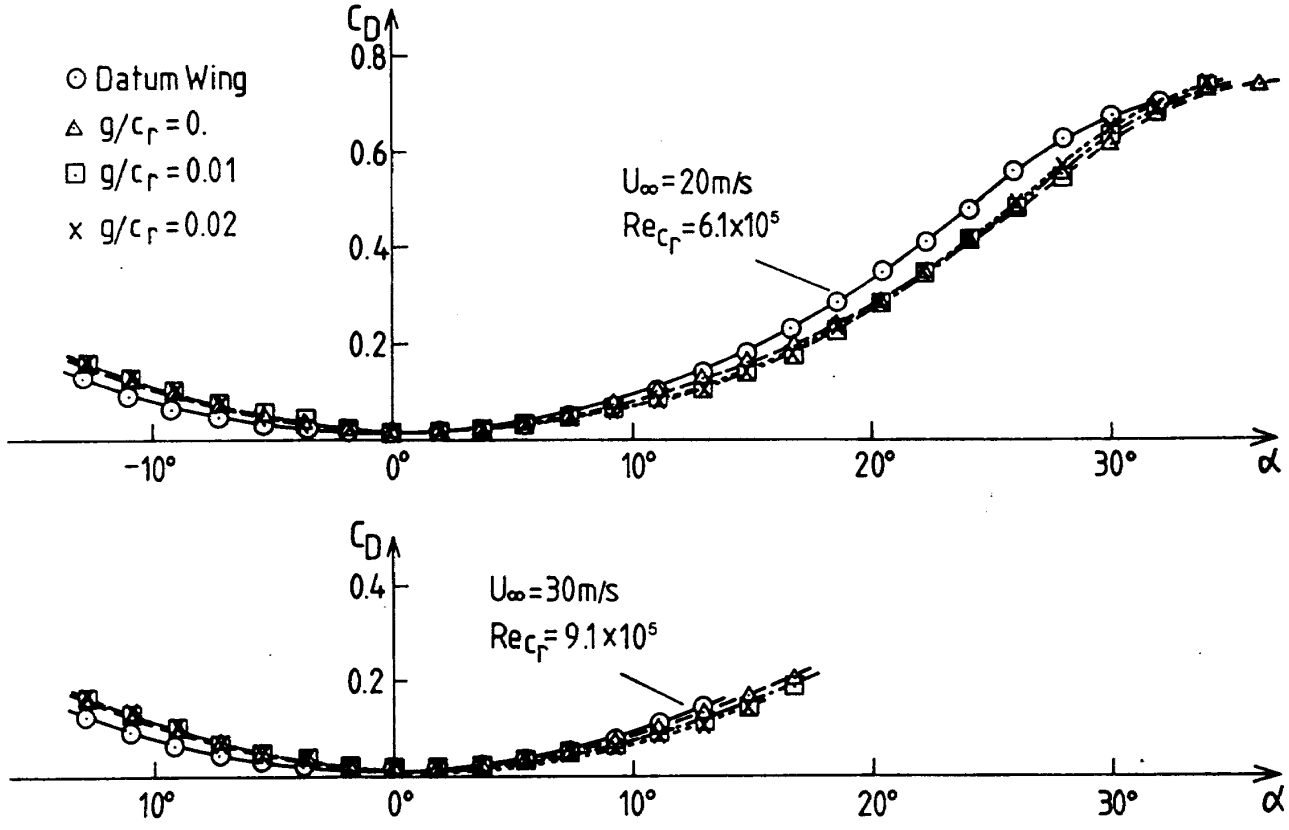

Fig. 13 Effect of Vortex Plate on C_D vs. α

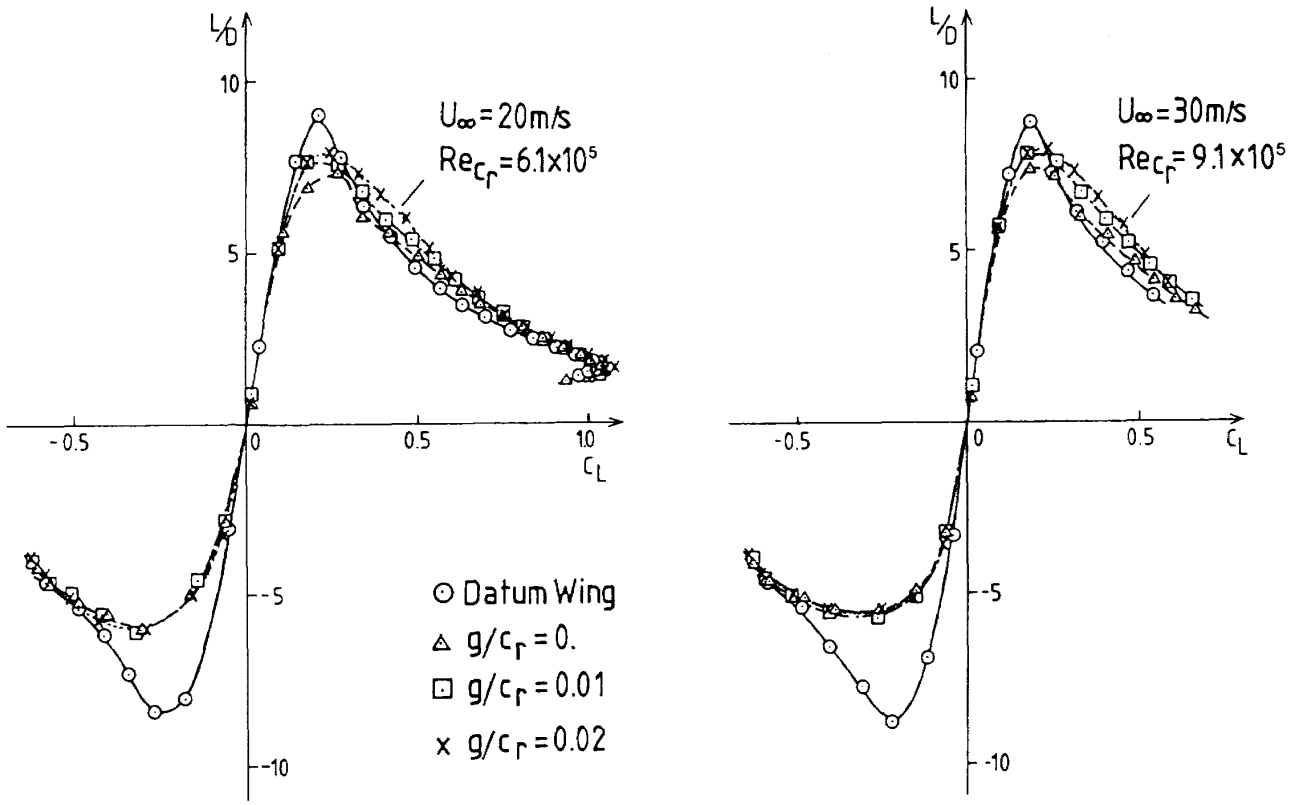

Fig. 14 Effect of Vortex Plate on *L/D* vs. C_L

does not affect the *L/D* value because this is a pure ratio of forces. When compared with the vortex flap results (Fig. 7), the *L/D* for $g/Cr = 0.02$ at C_L's greater than 0.35 is roughly comparable to that of the vortex flap deflected 30° downward.

Fig. 15 sketches the upper surface oil flow patterns for the datum wing, with and without a vortex plate, at incidences from 3.7° to 22.3°. The Reynolds number was 6.1×10^5. From this figure it is seen that the onset of the leading-edge separation vortex is between $\alpha = 3.7°$ and 5.5° for the datum wing, at $\alpha = 5.5°$ for $g/Cr = 0$, at $\alpha = 7.3°$ for $g/Cr = 0.01$ and at $\alpha = 9.2°$ for $g/Cr = 0.02$. This means that the onset of the leading-edge separation vortex is delayed by the vortex plate, the delay increasing as g/Cr increases.

Fig. 16 gives some indication of the leading-edge suction recoverable through vortex plate deployment. The maximum drag which corresponds to no leading-edge suction is:

$$C_D = C_{D0} + C_L \cdot \tan \alpha,$$

where C_{D0} is the zero-lift drag, which depends on the surface skin friction and the form drag. On the other hand, a wing with a well rounded leading-edge and no flow separation could have a drag coefficient described by:

$$C_D = C_{D0} + KC_L^2/(\pi AR),$$

where AR is the aspect ratio and $(KC_L^2/(\pi AR))$ is the lift induced drag for attached flow with 100% leading-edge suction. $K = 1.014$ is estimated from ESDU data sheets (ref. 12). Using the C_{D0} measured in the present tests, C_D for the 0% and the 100% leading-edge suction are plotted as C_D vs. α curves for the datum wing (Fig. 16a) and $g/Cr = 0.02$ (Fig. 16b). In order to plot the 100% leading-edge suction on C_D vs. α curves in Fig. 16, it was assumed that $(dC_L/d\alpha)$ is equal to the measured value. For the datum wing, the measured value agrees with 0% leading-edge suction value quite well for $0° < \alpha < 20°$ region. For $g/Cr = 0.02$ the measured value is less than the 0% leading-edge suction case for $0° < \alpha < 30°$ region, which suggests that by incorporating the vortex plate some leading-edge suction is recovered. This reduces the C_D as was seen in Fig. 13 and improves the *L/D* ratio as was seen in Fig. 14. Ref. 9 suggested the existence of a separation

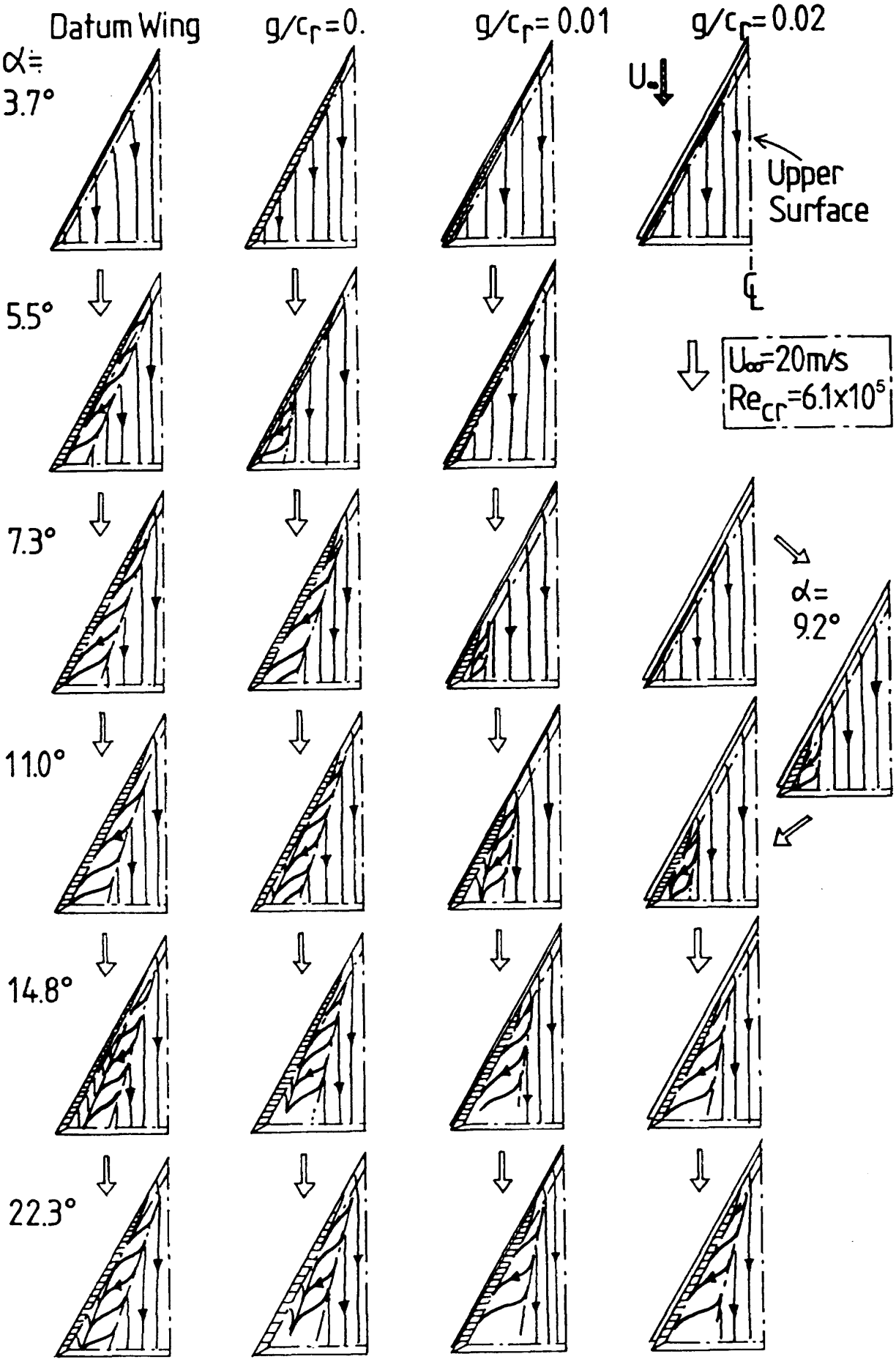

Fig. 15 Surface Flow Patterns with and without Vortex Plate

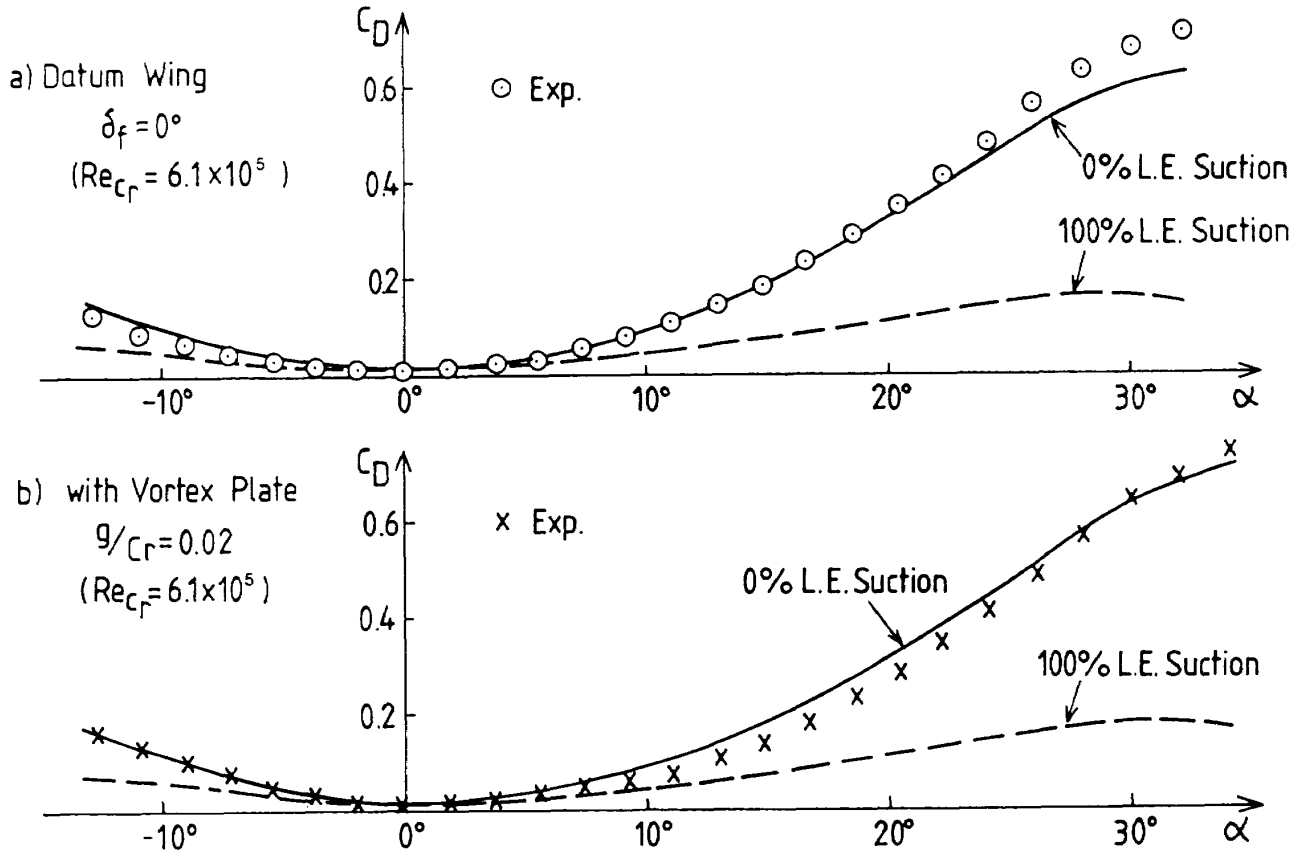

Fig. 16 Effect of Leading-Edge Suction Force on C_D (Datum Wing & $g/Cr = 0.02$)

vortex between the leading-edge of the wing and that of the vortex plate, but the smoke filament visualization tests here did not confirm the existence of a vortex. However, it seems that a separated flow acting on the forward facing region between the vortex plate and the wing produces some leading-edge suction force.

4. Conclusions

Lift and drag measurements were made at Reynolds numbers of 6.1×10^5 and 9.1×10^5 based on the centreline chord. The results showed that there are no major differences between the two sets of tests.

1) The L/D ratio reaches a maximum for any given flap defection angle when the flow comes smoothly onto the vortex flap without forming a large separation vortex over the flap surface, as was suggested in ref. 7. The highest $(L/D)_{max}$ was achieved at a flap deflection angle of 10°.
2) At high incidences a leading-edge separation vortex is formed on the LEVF surface at every flap deflection angle. Because of the suction effect of this separation vortex, the L/D is higher than that of the datum wing, as was suggested in ref. 1.
3) By incorporating the inverted vortex flap, both the lift and the drag can be increased above the datum wing values at the same incidence. However the L/D ratio is reduced.
4) By incorporating the vortex plate, the L/D ratio for all ranges of C_L greater than 0.3 is significantly improved. The vortex plate performance for $g/Cr = 0.02$ is roughly comparable to that of the vortex flap deflected 30° downward. The measured C_D suggests that some leading-edge suction acts on the wing and so reduces the drag. The occurrence of the leading-edge separation vortex on the wing is delayed when a protruding vortex plate is used.

Acknowledgement

The author expresses his appreciation to Professor J.L. Stollery, College of Aeronautics, for his advice

and guidance in carrying out this research. He also thanks members of the aerodynamics department workshop in Cranfield for their help in performing the wind tunnel experiments.

References

1) Rao, D.M. Leading Edge Vortex-Flap Experiments on a 74 deg. Delta Wing, NASA CR-159161, 1979.
2) Rao, D.M. Leading-Edge 'Vortex Flaps' for Enhanced Subsonic Aerodynamics of Slender Wings, ICAS-80-13.5, 1980.
3) Marchman III, J.F. Effectiveness of Leading-Edge Vortex Flaps on 60 and 75 Degree Delta Wings, J. Aircraft, Vol. 18, No. 4, pp. 280-286, 1981.
4) Campbell, J.F. and Osborn, R.F. Leading-Edge Vortex Research: Some Nonplanar Concepts and Current Challenges, NASA CP-2416, pp. 31-63, 1986.
5) Ellis, D.G. The Behaviour and Performance of Leading Edge Vortex Flaps, College of Aeronautics Report No. 8601, Cranfield, Feb. 1986.
6) Ellis, D.G. and Stollery, J.L. The Behaviour and Performance of Leading-Edge Vortex Flaps, ICAS-88-4.5.2, 1988.
7) Stollery, J.L. and Ellis, D.G. The Behaviour and Performance of Vortex Flaps, College of Aeronautics Report No. NFP8914, Cranfield, Nov. 1989.
8) Marchman III, J.F. Aerodynamics of Inverted Leading-Edge Flaps on Delta Wings, J.Aircraft, Vol. 18, No. 12, pp. 1051-1056, 1981.
9) Rao, D.M. and Johnson Jr., T.D. Investigation of Delta Wing Leading-Edge Devices, J. Aircraft, Vol.18, No.3, pp. 161-167, 1981.
10) Rae Jr., W.H. and Pope, A. Low-Speed Wind Tunnel Testing (2nd Ed.), John Wiley & Sons, New York, 1984.
11) Pankhurst, R.C. and Holder. D.W. Wind-Tunnel Technique; an Account of Experimental Methods in Low- and High-Speed Wind Tunnels, PITMAN, London, 1952.
12) ESDU. Subsonic Lift-Dependent Drag due to the Trailing Vortex Wake for Wings without Camber or Twist, Engineering Sciences Data Unit Item, No.74035, London, 1974.

既 刊 報 告

TR-1130	液体酸素ターボポンプ用セグメントシールの密封特性 Sealing Characteristics of a Curbon Segmented Circumferential Seal for a Liquid Oxygen Turbopump	1991年11月	尾池 守, 渡辺 義明 菊池 正孝, 野坂 正隆
TR-1131	ロケット用小型LH_2ポンプの研究試作(その3)流力性能 An Experimental Study of a Small High-Speed LH_2 Pump for Rocket 3rd Report; Fluid dynamic Performance	1991年11月	山田 仁, 渡辺 義明 平田 邦夫
TR-1132	視覚センサーとしてのビデオカメラ Video camera as a visual sensor	1991年11月	五味 広美
TR-1133	多孔板に対する音響インピーダンスモデルの評価 Evaluation of Acoustic Impedance Models for a Perforated Plate	1991年12月	渡辺 実
TR-1134	双発 USB 半裁模型風洞試験 Wind Tunnel Investigation of a Twin-Engine Jet Transport Semi-span Model with Upper Surface Blown Jet Flap	1991年12月	高橋 侔, 藤枝 郭俊 岩崎 昭人, 藤田 敏美 斉藤 雅樹
TR-1135	微分型センサ導入による運動推定精度の向上 Accuracy Improvement of Linear Estimated Motion Using Differential Type Sensors	1991年12月	佐々 修一, 永安 正彦 柳原 正明, 下村 卓
TR-1136	液晶型フラット・パネル・ディスプレイのシミュレータ評価試験 その2:Dサイズ型 PFD, DMD Flight Simulator Evaluation of D-size Liquid Crystal Flat Panel Displays	1991年12月	川原 弘靖, 若色 薫 渡辺 顯
TR-1137	マッハ4におけるスクラムジェット空気取入口の実験(その1) Mach 4 Testing of Scramjet Inlet Models(I)	1991年12月	苅田 丈士, 小室 智幸 升谷 五郎, 工藤 賢司 村上 淳郎, 谷 香一郎 若松 義男, 鎮西 信夫
TR-1138	低騒音STOL実験機「飛鳥」の動的飛行試験による空力モデル同定 Aerodynamic Model Identification of Quiet STOL Experimental Aircraft "ASKA" from Dynamic Flight Test Data	1992年1月	STOLプロジェクト 推進本部飛行試験室
TR-1139	多元連立1次方程式に対する反復計算法の改良について Improvements for Obtaining Iterative Solutions of Large Linear Systems	1992年2月	西村 英明

TECHNICAL REPORT OF NATIONAL AEROSPACE LABORATORY
TR-1140T

航空宇宙技術研究所報告1140T号(欧文)

平成4年3月発行

発行所 航空宇宙技術研究所
東京都調布市深大寺東町7丁目44番地1
電話三鷹(0422)47-5911(大代表)〒182
印刷所 株式会社 東京プレス
東京都板橋区桜川2-27-12

Published by
NATIONAL AEROSPACE LABORATORY
7-44-1 Jindaijihigashi-Machi Chōfu, Tokyo
JAPAN

Printed in Japan